









RESEARCH ARTICLE | AUGUST 19 2024

Photothermal phase modulation in a gas-immersed optical nanofiber

Hanyu Liao ; Yun Qi ; Shoulin Jiang ; Hoi Lut Ho ; Haihong Bao  ; Wei Jin  *Appl. Phys. Lett.* 125, 082201 (2024)<https://doi.org/10.1063/5.0217776>

Applied Physics Letters

Special Topics Open for Submissions

[Learn More](#)

Photothermal phase modulation in a gas-immersed optical nanofiber

Cite as: Appl. Phys. Lett. **125**, 082201 (2024); doi: [10.1063/5.0217776](https://doi.org/10.1063/5.0217776)

Submitted: 31 May 2024 · Accepted: 6 August 2024 ·

Published Online: 19 August 2024



View Online



Export Citation



CrossMark

Hanyu Liao,^{1,2} Yun Qi,^{1,2} Shoulin Jiang,^{1,2} Hoi Lut Ho,^{1,2} Haihong Bao,^{1,2,a)} and Wei Jin^{1,2,a)}

AFFILIATIONS

¹Department of Electrical and Electronic Engineering and Photonics Research Institute, The Hong Kong Polytechnic University, Hong Kong, China

²Photonics Research Center, The Hong Kong Polytechnic University Shenzhen Research Institute, Shenzhen, China

^{a)}Authors to whom correspondence should be addressed: haihong.bao@polyu.edu.hk and wei.jin@polyu.edu.hk

ABSTRACT

We report the observation and theoretical analysis of photothermal phase modulation in an optical nanofiber (NF) immersed in light-absorbing gas. The phase modulation arises from the contrasting photothermal processes experienced by the mode field within and outside the NF, which exhibits significant wavelength and pressure dependence in the nanoscale waveguides. By designing the diameter of the NF, the photothermal phase modulation can be readily controlled, and a nullification of phase modulation is achieved at a specific wavelength. Experiments on NFs with different diameters demonstrated pressure-controllable phase modulation up to 0.058π rad/mW, potentially allowing the development of nanoscale all-optical modulators and sensors with optimal performance.

© 2024 Author(s). All article content, except where otherwise noted, is licensed under a Creative Commons Attribution-NonCommercial-NoDerivs 4.0 International (CC BY-NC-ND) license (<https://creativecommons.org/licenses/by-nc-nd/4.0/>). <https://doi.org/10.1063/5.0217776>

Optical nanofiber (NF) has emerged as a promising platform for efficient light-matter interaction due to its subwavelength scales, which offer a reduced mode field area with an open evanescent field extending beyond the core boundary. The highly constrained evanescent field provides diverse possibilities for the functionalization of NFs with enhanced interaction efficiency. There have been reports of highly efficient two-photon absorption,¹ electromagnetically induced transparency,² stimulated Brillouin effect,³ and stimulated Raman effect⁴ based on NFs coupled with different mediums. However, when the diameter of the NF is much smaller than the wavelength, the light confinement of the NF would dramatically decrease, leading to a significantly increased mode field area with much reduced optical power density,⁵ which can even support a super-extended mode.⁶ This behavior is particularly evident in these thin core NFs, making the mode field distribution highly sensitive to the optical wavelength and more interactive with the outside medium. For nonlinear interactions in NF, this characteristic requires a balance between the mode field area and the power density to achieve the maximum interaction efficiency.^{4,7} For linear interactions, a smaller core diameter is preferred so that a higher proportion of optical field could extend outside to drive the interaction,⁸ but it also leads to a considerable wavelength dependence of the fractional evanescent power, which is typically 0.1% per nm.⁹ A large overlap between the optical field and the medium may also alter

the mode profile and induce high propagation loss, especially for solid materials with intrinsic backscattering and broadband absorption.

Here, we report the observations of photothermal phase modulation in thin core NFs immersed in light-absorbing gas, which exhibits a marked sensitivity to both wavelength and gas pressure. Gas has much narrower absorption lines and lower backscattering, enabling extremely small core NF-based devices with a large light-gas overlap for a broad wavelength range. The gas absorption of a control beam generates heat, which modulates the refractive index (RI) of the gas and NF materials and hence the phase of another signal beam. Since the RI changes of gas and solid core (i.e., silica) have opposite signs, the overall phase modulation is highly sensitive to the mode field distribution in the NFs, of which the wavelength dependence could be significant. By changing the core diameter and adjusting the gas pressure, the wavelength dependence can be selectively enhanced or nullified to meet the demands of different applications. A theoretical model describing this phenomenon is present and verified by experiments, which provides a guideline for the selection of the NF diameter and gas pressure for optimal performance.

Figure 1(a) illustrates the basics of the photothermal phase modulation in a gas-immersed optical NF. A control beam with its wavelength tuned to a gas absorption line co-propagates with a signal beam in the NF. Both beams have strong evanescent fields extending into the

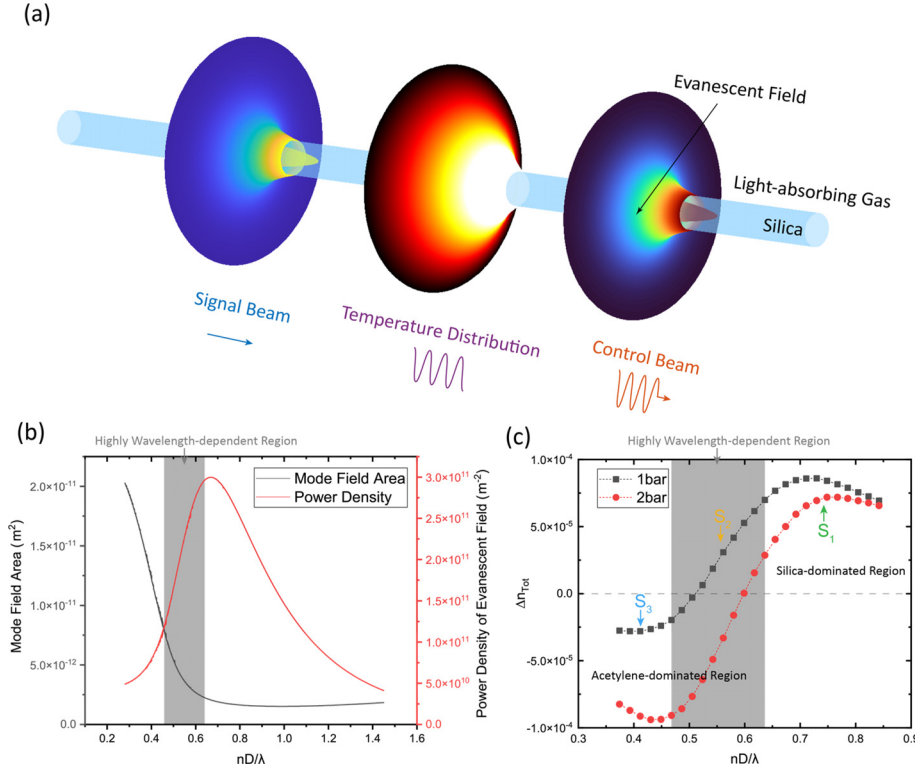


FIG. 1. Illustration of photothermal phase modulation in an NF immersed in gas. (a) Schematic of the photothermal effect in NF. Gas absorption of the evanescent field of the intensity-modulated control beam modulates the temperature distribution and is perceived by the signal beam. (b) Calculated mode field area and equivalent power density of evanescent field for different normalized NF diameter. The equivalent power density is defined as the power fraction of the evanescent field divided by the mode field area. The shaded region denotes the region where the evanescent power density changes most rapidly. (c) Simulated photothermal phase modulation on signal beam for different normalized NF diameter under 1 bar/2 bar gas pressure. The control beam is assumed to be 200 mW and is intensity-modulated at 20 kHz. The photothermal phase modulation varies fastest with wavelength in the shaded region, corresponding to the shaded region in (b) where the equivalent power density change is fastest. S1, S2, and S3 denote the NF samples with different diameters that are tested in our experiments. The dotted line marks the situation where $\Delta n_{tot} = 0$, and the effects of gas and silica cancel out.

gas medium surrounding the NF. Gas molecules absorb the power of the control beam with a coefficient α in cm^{-1} , resulting in heat generation due to non-radiative relaxation. The heat generation leads to the modulation of temperature distribution in gas and silica through thermal conduction, which consequently modulates the phase of the signal beam via the thermo-optic (TO) effect of the materials (gas and silica) and the thermal expansion (TE) effect of the silica waveguide.¹⁰ Take silica NF in pure acetylene as an example, for a sinusoidally intensity-modulated pump beam, the phase modulation of the signal is also sinusoidal with the same frequency and the peak-to-peak amplitude of the phase modulation may be expressed as (see S1 of the [supplementary material](#) for the complete theory)

$$\begin{aligned} \Delta\phi_{pp} &= \phi(T_{\max}) - \phi(T_{\min}) \\ &\approx \frac{2\pi}{\lambda_s} \int_0^L \left(\underbrace{e_s^{TE} \bar{n}_{eff} \Delta T(z)}_{\text{Length change}} + \underbrace{\Delta n_{eff}^{TE}(z)}_{\text{Radius change}} + \underbrace{\Delta n_{eff}^{TO}(z)}_{\text{RI change}} \right) dz \\ &:= \frac{2\pi}{\lambda_s} \int_0^L \Delta n_{tot}(z) dz, \end{aligned} \quad (1)$$

where $\Delta\phi_{pp}$ is the peak-to-peak phase modulation amplitude of the signal beam, $T_{\max, \min}$ are the peaks and troughs of the time-oscillating temperature field, λ_s is the wavelength of the signal beam, L is the length of the NF, $\Delta T(r, \theta)$ is the amplitude of the time-oscillating temperature field, and e_s^{TE} is the TE coefficient of silica.¹¹ Δn_{eff} is the modulation of effective mode index at the signal wavelength, and the superscript denotes the origin of the modulation. Δn_{tot} is the

equivalent mode RI change of the photothermal phase modulation and comprises three terms. The first term represents the integrated effect of the longitudinal TE effect along the length of the NF, from which the phase change is proportional to temperature rise. The second term represents the contribution of the transverse TE effect of the NF and is also consistently positive to temperature rise, as a higher temperature leads to an increase in the radius of the NF and hence a larger effective RI of the signal mode. The third term accounts for the contribution of the TO effect of materials and is much larger than the first two terms, the sign of which, however, is decided by the mode field distribution of the signal beam and the gas pressure,^{12,13}

$$\begin{aligned} \Delta n_{eff}^{TO} &= \iint \Delta T(r, \theta) \left(-\frac{\mu p}{T(r, \theta)^2} \psi_s(r > \bar{r}_s, \theta) \right. \\ &\quad \left. + e_s^{TO} \psi_s(r < \bar{r}_s, \theta) \right) r dr d\theta, \end{aligned} \quad (2)$$

where ψ_s is the normalized mode field distribution of the signal beam, \bar{r}_s is the radius of the core at average temperature, μ is the specific refractivity of gas, p and $T(r, \theta)$ are the pressure and temperature, and $e_s^{TO} = 8.5 \times 10^{-6} \text{K}^{-1}$ is the TO coefficient of silica.¹⁴ The term $-\mu p/T^2$ is the TO coefficient of gas,¹⁵ whose negative sign denotes the mode field outside the core experiences opposite the RI change compared with the inside. As depicted by Eq. (2), the efficiency of the photothermal phase modulation depends on the gas pressure. For a thinner NF, the evanescent field in gas [$\psi_s(r > \bar{r}_s, \theta)$] has a larger portion, leading to the dominance of the TO effect of gas and making it more sensitive to pressurization.

The wavelength dependence of the photothermal phase modulation $\Delta\phi_{pp}$ originates from the TO term in Eq. (1), which directly depends on the signal field distribution ψ_s . A slight shift in the signal wavelength from longer to shorter would alter the ψ_s to have a larger proportion outside the core radius, resulting in an increased TO effect of gas and a reduced TO effect of silica, as described by Eq. (2). Therefore, the wavelength dependence of the mode field significantly impacts the phase modulation in the thin core NFs according to the interplay of the opposite TO effect of gas and silica (see S2 of the [supplementary material](#) for details). Figure 1(b) shows the mode field area (A_{eff}) and the equivalent power density⁴ (kA_{eff}^{-1}) of the evanescent field for different normalized NF diameter nD/λ , where k is the power fraction of the evanescent field. As shown in Fig. 1(c), the photothermal phase modulation changes fastest in the shaded region, corresponding to the fastest change of the equivalent power density in the shaded region of Fig. 1(b). To further discuss the characteristics of the photothermal phase modulation, we categorize three distinct regions through Fig. 1(c). For a thin core NF diameter with a much-extended evanescent field, the photothermal phase modulation is dominated by the TO effect of the gas, causing the mode phase to decrease with the temperature rise; we accordingly defined it as the acetylene-dominated region. For an NF with a considerably larger diameter, the mode field is tightly constrained in the fiber core and leads to a dominance of silica TO effect; hence, termed as silica-dominated region where the mode phase increases with the temperature rise. The third region lies between the first two and is a highly wavelength-dependent region, where the equivalent power density of the evanescent field changes quickly with wavelength, resulting in a high sensitivity of the mode phase modulation to the wavelength changes. Note that the wavelength dependence is also controllable by changing the gas pressure, as a higher pressure leads to a larger TO effect of gas.

As examples, we fabricated three different NF samples S_1 , S_2 , and S_3 with ~ 10 mm waist length NF and ~ 0.79 , ~ 0.66 , and ~ 0.44 μm diameters, respectively. Their diameter-to-wavelength ratio is marked in Fig. 1(c), corresponding to silica-dominated region, highly wavelength-dependent region, and acetylene-dominated region, respectively. We sealed the NFs into quartz capillaries filled with pure

acetylene to prevent external contamination, and one of the sealed capillaries (Sample S_2) is shown in Fig. 2(a) together with its typical transmission loss spectrum. The insertion loss of the device is in general smaller than 0.8 dB over the wavelength range of 1450–1650 nm, except the around the acetylene absorption lines. The NFs are then characterized by the setup shown in Fig. 2(b). The control beam is from a distributed feedback (DFB) laser with a wavelength of 1532.83 nm, aligned to the P(13) absorption line of acetylene. The signal beam comes from an external cavity diode laser (ECDL) and is combined with the control beam and launched into the NF. To evaluate the phase modulation, a Mach-Zehnder interferometer (MZI) is built with the NF placed in the measurement arm. In the reference arm, an SMF is coiled around a piezoelectric transducer (PZT), which is used to maintain the operation of the MZI at phase quadrature via a servo-loop. A tunable fiber coupler (TFC) is used as the input splitter to maximize the fringe contrast. The signal beam is phase-modulated by the photothermal effect in the gas-immersed NF and transformed into an intensity modulation at the MZI output, which is detected by a photodetector (PD₁) and observed using an oscilloscope (OSC₁).

We first evaluate the general photothermal phase modulation characteristics of sample S_2 . Figure 3(a) shows the output waveform with the MZI locked at the quadrature point when the modulation frequency of the control beam is set at 1 kHz. The corresponding phase modulation amplitude can be calculated based on the waveforms.¹⁶ Figure 3(b) shows the calculated phase modulation amplitude for 1, 10, and 100 kHz, which increases linearly with control power (P_c). The measured frequency response is shown in Fig. 3(c), and the 3-dB bandwidth is 9 kHz. We also studied the transient response of the NFs to square control pulses with a duty cycle of 50% at the repetition rate of 10 kHz; the result is shown in Fig. 3(d). By fitting to exponential functions, the rise and fall time of S_2 are determined to be 7.9 and 8.4 μs , respectively, which is an order of magnitude faster than the previously reported photothermal phase modulators based on micro/nanofibers coated with solid materials.^{17–19} The fast response is attributed to the high surface-area-to-volume ratio (SA:V) of the thin core NF and the high spatial overlap of the signal field with the heat source. On the one hand, the heat generated is highly localized around the surface of the

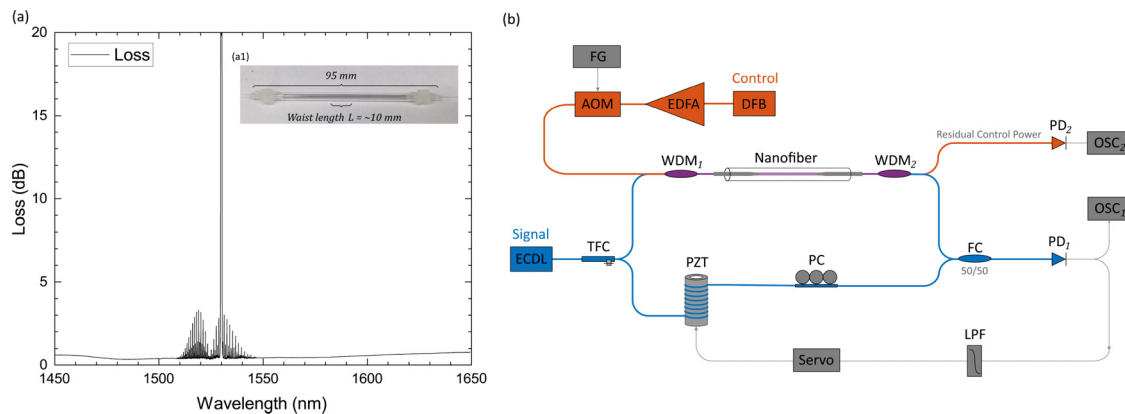


FIG. 2. (a) Measured transmission loss spectrum of the sample S_2 . The inset (a1) shows the picture of an NF housed in a capillary filled with acetylene. (b) The experimental setup for testing the NFs. EDFA: erbium-doped fiber amplifier, for amplifying the control beam; AOM: acoustic-optic modulator, for intensity modulation on the control beam; WDM: wavelength division multiplexer; PC: polarization controller, for optimizing the fringe contrast; FC: fiber coupler; FG: function generator for driving the AOM; LPF: low pass filter, for limiting the feedback frequency bandwidth.

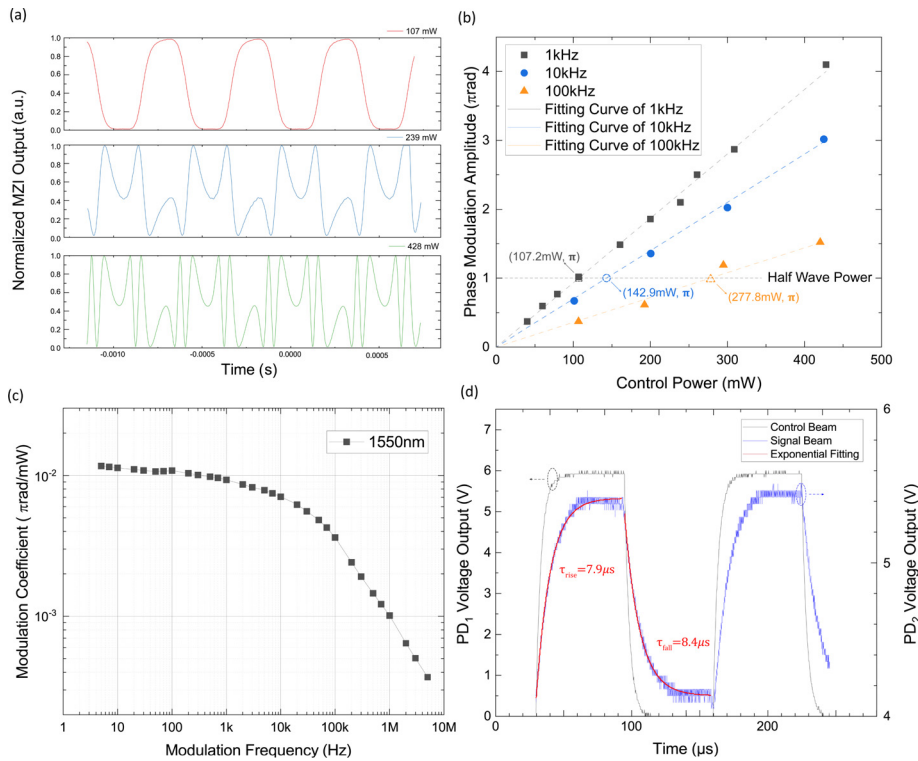


FIG. 3. Phase modulation characteristics of S_2 at 1 bar. (a) Measured waveform with control power at 107, 239, and 428 mW at 1 kHz, respectively. (b) Phase modulation amplitude as a function of control power for three different modulation frequencies. The hollow points show the half-wave control power at the corresponding modulation frequencies. (c) Frequency response of phase modulation. (d) Transient response of the phase modulation with periodic on/off control beam. The red line shows the exponential fit of rising and falling edges.

NF due to the tight confinement of the control beam, which can be quickly transported to the interior of the NF due to the high SA:V and high thermal conductivity of silica; on the other hand, the evanescent field of signal beam is also tightly confined and coincide with the control beam in space, even though the thermal conductivity of acetylene is relatively low, the response is not strongly affected by the rate of heat conduction of acetylene away from the NF. It could also be theoretically proved that the response time of the photothermal phase modulation is inversely proportional to the equivalent heat conduction area A_{eq} as $\tau_r \approx 2.2\rho_a c_a A_{eq}/k_a$, where ρ , c , a and k are the density, heat capacity, and thermal conductivity of the acetylene, respectively (see

S3 in the [supplementary material](#) for details). As a proof of principle, the measured rise and fall time of the thicker NF sample S_1 , which has a larger diameter than S_2 , are determined to be 55.2 and 43.7 μ s.

We then compare the wavelength dependence of the photothermal phase modulation among the three samples at different gas pressures. Figure 4 shows the measured phase modulation efficiency of the three NFs. Sample S_1 demonstrates lower efficiency in photothermal phase modulation at higher gas pressure as it is dominated by the TO effect of silica. In contrast, S_3 positions in the acetylene-dominated region in Fig. 1(c), the measured phase modulation is significantly enhanced through pressurization and with much reduced wavelength

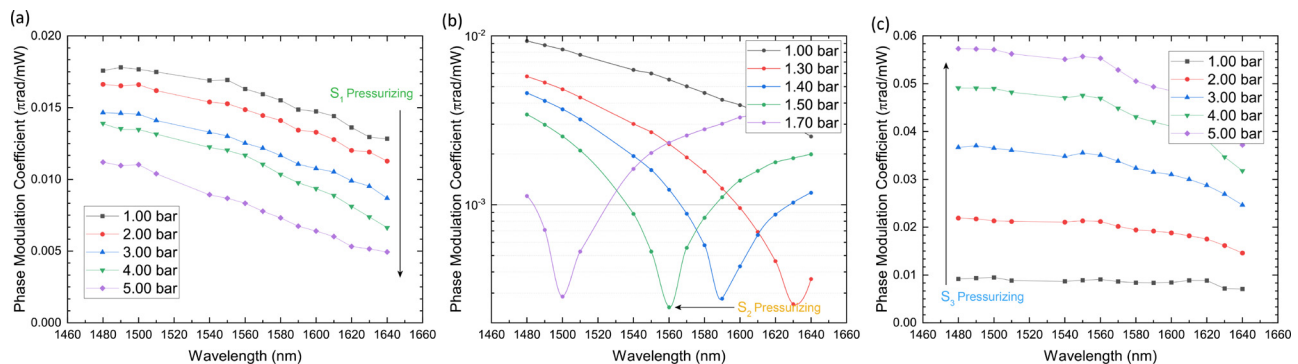


FIG. 4. Wavelength dependence of NFs with diameters of (a) 0.76 μ m (S_1), (b) 0.66 μ m (S_2), and (c) 0.44 μ m (S_3), corresponding to silica-dominated region, highly wavelength-dependent region, and acetylene-dominated region, respectively. The control beam is intensity modulated at 20 kHz. The wavelength dependences of the three samples are all increased with gas pressure, which is attributed to the change of the TO effect of gas.

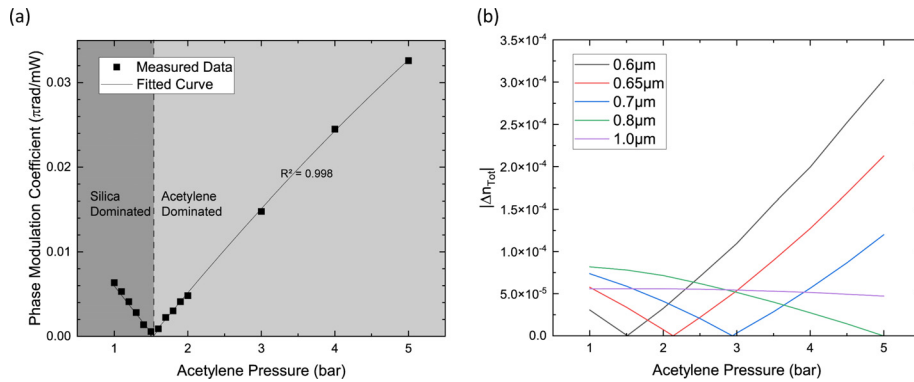


FIG. 5. Pressure dependence of the photothermal phase modulation for sample S2 immersed in pure acetylene. (a) Experimental results. The solid line is a polynomial fitting of the measured data. (b) Simulation results of the effective mode index modulation $|\Delta n_{tot}|$. The control power is 200 mW with intensity modulated at 20 kHz. The signal wavelength is 1550 nm.

dependence, the slope of which is five times smaller than sample S₁ at 1 bar. Sample S₂, which is situated at the high wavelength-dependent region, exhibits a remarkable nullification window of the photothermal phase modulation, of which the modulation efficiency at the center is 11 dB smaller than that of the wavelength outside the window. The center wavelength of the nullification window is sensitive to the gas pressure with a coefficient of 0.275 nm/mbar, which makes it widely tunable in the whole S + C + L band. The highest photothermal phase modulation is 0.058 π rad/mW achieved by S₃ under 5 bar gas pressure, which could be further improved with higher pressure and longer NF.

We further examine the pressure dependence of the photothermal phase modulation for the high wavelength-dependent sample S₂ with signal wavelength fixed at 1550 nm. The results are shown in Figure 5. At low gas pressure, the phase modulation is dominated by the TO effect of silica, which is gradually canceled out and replaced by the TO effect of gas through pressurization. Note that the Kerr effect contributes $\sim 0.37\%$ of the total phase modulation in our experiment, which has been subtracted in calculating the photothermal phase modulation coefficient. Figure 5(b) shows the simulated effective RI change with pressure for NFs with different NF diameters. For a thinner NF, the evanescent field has a larger portion, leading to the dominance of the TO effect of gas and making it more sensitive to pressurization, which is in good agreement with the experiment.

In conclusion, we have reported the photothermal phase modulation on thin core NF immersed in light-absorbing gas, which is highly sensitive to wavelength and gas pressure. The sensitivity to signal wavelength arises from the inherent wavelength dependence of the mode field distribution in thin core NF, which accordingly affects photothermal phase modulation by altering the ratio of the TO effect of gas and silica. The gas medium imparts the pressure sensitivity to the photothermal phase modulation, rendering both its magnitude and wavelength dependence highly customizable. Distinct behaviors of the photothermal phase modulation are observed experimentally by silica NFs of varying core diameters immersed in pure acetylene. A small core NF with a diameter of $\sim 0.44 \mu\text{m}$ allows a significant enhancement of the photothermal phase modulation through pressurization, achieving an efficiency of 0.058 π rad/mW under a 20 kHz control at 5 bar pressure. Conversely, a larger core diameter of $\sim 0.79 \mu\text{m}$ shifts the phase modulation dominance to silica, thereby reducing the efficiency upon pressurization. An intermediate core diameter of $\sim 0.66 \mu\text{m}$ presents a unique nullification window at a specific wavelength that is highly sensitive to gas pressure, with a coefficient of 0.275 nm/mbar.

As compared to previously reported solid materials,^{18,20,21} the gas-based photothermal phase modulation offers advantages such as adjustable modulation efficiency, low backward scattering loss, high damage threshold, and microsecond-level response time. The wavelength-dependent photothermal phase modulation can also be achieved based on other light-absorbing gas or gas mixtures with carefully designed nD/λ to operate effectively in the high-wavelength dependent region. Different fiber materials and types of nanowaveguides²² could also be utilized to extend the operation at ultra-violet, visible, or infrared wavelength bands. To meet the requirements of various applications, it is essential to achieve higher phase modulation efficiency and shorter response time when designing the photothermal phase modulation systems under different waveguides and gases. The maximum modulation efficiency is found approximately proportional to $\alpha L e_{eff}^{TO}/k_a$ (see S3 of the supplementary material), while the response time $\tau_r \approx 2.2 \rho_a c_a A_{eq}/k_a$. The highly customizable gas-assisted photothermal phase modulation in NF, with its significant sensitivity to pressure and wavelength, holds great potential for the development of gas-based all-optical nanodevices, such as phase modulator²³ and gas and pressure sensors.^{10,24}

See the supplementary material for the detailed theory of photothermal phase modulation in gas-immersed NF (S1), the origin of the wavelength dependence (S2), and the approximated solution for heat transfer equation (S3). The contributions of the TO and TE effects to the total phase modulation efficiency is formulated and numerically simulated. The wavelength dependence of the TO effect is discussed. The approximated solution of the heat transfer in gas-immersed NF provides a qualitative evaluation on the performance of the photothermal phase modulation.

This work was supported by the National Natural Science Foundation of China (Grant No. 62005233), the Local Innovative and Research Teams Project of Guangdong Pear River Talents Program (No. 2019BT02X105), the Shenzhen STIC Funding (No. RCB20200714114819032), and the Hong Kong Polytechnic University (Grant Nos. 1-YXAB, 1-W151, and 1-ZVY4).

AUTHOR DECLARATIONS

Conflict of Interest

The authors have no conflicts to disclose.

Author Contributions

Hanyu Liao: Conceptualization (equal); Data curation (equal); Formal analysis (equal); Investigation (equal); Methodology (equal); Software (equal); Validation (equal); Visualization (equal); Writing – original draft (equal); Writing – review & editing (equal). **Yun Qi:** Conceptualization (equal); Data curation (equal); Formal analysis (equal); Investigation (equal); Methodology (equal); Software (equal); Supervision (equal); Validation (equal); Writing – review & editing (equal). **Shoulin Jiang:** Funding acquisition (equal); Project administration (equal); Resources (equal). **Hoi Lut Ho:** Funding acquisition (equal); Project administration (equal); Resources (equal); Supervision (equal). **Haihong Bao:** Funding acquisition (equal); Resources (equal); Supervision (equal); Writing – review & editing (equal). **Wei Jin:** Funding acquisition (equal); Investigation (equal); Project administration (equal); Resources (equal); Supervision (equal); Writing – review & editing (equal).

DATA AVAILABILITY

The data that support the findings of this study are available from the corresponding authors upon reasonable request.

REFERENCES

- ¹S. Hendrickson, M. Lai, T. Pittman, and J. Franson, *Phys. Rev. Lett.* **105**(17), 173602 (2010).
- ²S. Spillane, G. Pati, K. Salit, M. Hall, P. Kumar, R. Beausoleil, and M. Shahriar, *Phys. Rev. Lett.* **100**(23), 233602 (2008).
- ³F. Yang, F. Gyger, A. Godet, J. Chrétien, L. Zhang, M. Pang, J.-C. Beugnot, and L. Thévenaz, *Nat. Commun.* **13**(1), 1432 (2022).
- ⁴Y. Qi, Y. Zhao, H. Bao, W. Jin, and H. L. Ho, *Optica* **6**(5), 570–576 (2019).
- ⁵L. Tong, J. Lou, and E. Mazur, *Opt. Express* **12**(6), 1025–1035 (2004).
- ⁶R. Finkelstein, G. Winer, D. Z. Koplovich, O. Arenfrid, T. Hoinkes, G. Guendelman, M. Netser, E. Poem, A. Rauschenbeutel, and B. Dayan, *Optica* **8**(2), 208–215 (2021).
- ⁷M. A. Foster and A. L. Gaeta, *Opt. Express* **12**(14), 3137–3143 (2004).
- ⁸M. J. Morrissey, K. Deasy, M. Frawley, R. Kumar, E. Prel, L. Russell, V. G. Truong, and S. N. Chormaic, *Sensors* **13**(8), 10449–10481 (2013).
- ⁹G. Y. Chen, M. Ding, T. Newson, and G. Brambilla, *Open Opt. J.* **7**(1), 33 (2013).
- ¹⁰Y. Qi, F. Yang, Y. Lin, W. Jin, and H. L. Ho, *J. Lightwave Technol.* **35**(24), 5267–5275 (2017).
- ¹¹W. H. Souder and P. Hidnert, *Measurements on the Thermal Expansion of Fused Silica* (US Government Printing Office, 1926).
- ¹²J. C. Owens, *Appl. Opt.* **6**(1), 51–59 (1967).
- ¹³P. E. Ciddor, *Appl. Opt.* **35**(9), 1566–1573 (1996).
- ¹⁴D. B. Leviton and B. J. Frey, Paper Presented at the Optomechanical Technologies for Astronomy, 2006.
- ¹⁵Y. Clergent, C. Durou, and M. Laurens, *J. Chem. Eng. Data* **44**(2), 197–199 (1999).
- ¹⁶W. Jin, D. Uttamchandani, and B. Culshaw, *Appl. Opt.* **31**(34), 7253–7258 (1992).
- ¹⁷X. Gan, C. Zhao, Y. Wang, D. Mao, L. Fang, L. Han, and J. Zhao, *Optica* **2**(5), 468–471 (2015).
- ¹⁸Q. Guo, K. Wu, Z. Shao, E. T. Basore, P. Jiang, and J. Qiu, *Adv. Opt. Mater.* **7**(13), 1900322 (2019).
- ¹⁹K. Wu, C. Guo, H. Wang, X. Zhang, J. Wang, and J. Chen, *Opt. Express* **25**(15), 17639–17649 (2017).
- ²⁰H. Chen, C. Wang, H. Ouyang, Y. Song, and T. Jiang, *Nanophotonics* **9**(8), 2107–2124 (2020).
- ²¹Y. Wang, W. Huang, J. Zhao, H. Huang, C. Wang, F. Zhang, J. Liu, J. Li, M. Zhang, and H. Zhang, *J. Mater. Chem. C* **7**(4), 871–878 (2019).
- ²²Q. Li, Y. Jia, L. Dai, Y. Yang, and J. Li, *ACS Nano* **9**(3), 2689–2695 (2015).
- ²³S. Jiang, F. Chen, Y. Zhao, S. Gao, Y. Wang, H. L. Ho, and W. Jin, *Opto-Electron. Adv.* **6**(5), 220085 (2023).
- ²⁴D. Kim, E. Lee, M. Cho, C. Kim, Y. Park, and T. Kouh, *Appl. Phys. Lett.* **102**(20), 203502 (2013).